

Enabling photodetection electronics for fluorescent diamond based quantum sensing

Vladislav Serafimov

November 6, 2025

Contents

1 Foreword	3
2 Summary	4
3 Introduction	5
3.1 Background	5
3.2 Purpose of the assignment	5
3.3 Assignment specifications	6
3.4 Scope of work	6
3.4.1 Project boundaries	6
3.4.2 Goals	7
3.4.3 Deliverables	7
3.5 Methodology	8
3.6 Report outline	8
4 Functional design	9
4.1 Background knowledge	9
4.1.1 Spin states	9
4.1.2 Zeeman effect	9
4.1.3 Energy levels	9
4.2 Quantum protocols	10
4.2.1 CW-ODMR	10
4.2.2 T_1 relaxometry	10
4.2.3 P-ODMR	12
4.3 Quantum sensing setup	12
4.4 Lock-in amplification	13
4.5 Photodetection	13
4.6 Photodiodes	13
4.6.1 Design process	14
5 Technical design	16
5.1 Quantum sensing setup	16
5.2 Photodetector design	16
5.2.1 First iteration	16
5.2.2 Second iteration	16
5.3 Photodetection implementation	17
5.3.1 First iteration	17
5.4 OLIA implementation	18
6 Testing results	20
6.1 Test goals and performance metrics	20
6.2 Test setup	21
6.3 Results and discussion	21
6.4 Known limitations	21
7 Conclusion	22
8 Recommendations	23
Appendices	24

A Code	24
Glossary	25

Chapter 1

Foreword

Chapter 2

Summary

Chapter 3

Introduction

This chapter introduces the assignment and some foundational concepts of quantum sensing.

3.1 Background

Nitrogen Vacancy (NV) centers [1] are imperfections in the atomic structure of diamonds. The two types of NV centers are NV0 and NV-, as seen in Figure 3.1, but the NV- structure is much more commonly used in quantum applications. These imperfections have the useful property of spin-dependent luminescence. This means that the spin of the NV center affects the frequency of the light emitted by the structure¹. Using this quality of the NV structure, different environmental metrics (e.g magnetic fields) can be measured.

The Applied Nanotechnology research group is working on a NV-center-based sensor setup. There exist several quantum protocols, but the one this setup needs to support is called Constant-Wave ODMR (ODMR). At its core, Optically Detected Magnetic Resonance (ODMR) is a set of protocols, which can detect magnetic fields based on the fluctuations in the fluorescence of NV centers [3]. CW-ODMR in particular involves exposing the NV center to a Microwave (MW) sweep while illuminating it with a constant light source. This is in contrast with Pulsed ODMR (ODMR) techniques, which use different Transistor-Transistor Logic (TTL) pulse schemes [4] to modulate the MW signal and the light source.

Processing data from the setup requires working with weak signals that are hard to distinguish from the environmental noise. While this is a significant problem, it is also a very common one. Because of this, there is already widely-used system used to isolate signals in such cases: the lock-in amplifier.

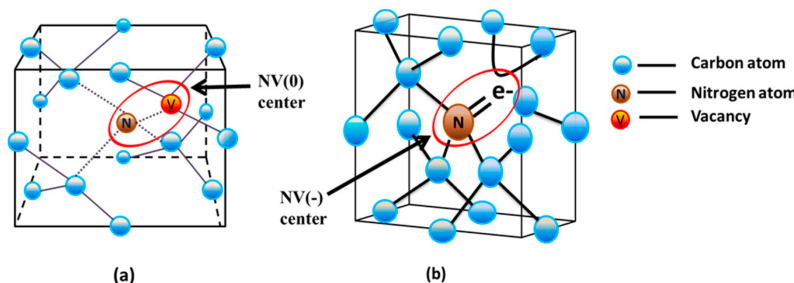


Figure 3.1: NV0 (a) and NV- (b) structures in diamonds (image credit to Haque et al [5])

3.2 Purpose of the assignment

Implementing a lock-in amplifier is the main purpose of the assignment. To create a complete solution, there are several different functionalities and systems that need to be developed.

Before doing anything else, the raw sensor data needs to be extracted and then fed to a lock-in amplifier. This should be done in a standardized manner, in order to facilitate testing with different devices. After establishing connection, a control interface needs to be implemented. It needs to

¹The NV center only emits light after absorbing photons, a phenomenon called photoluminescence [2]

be programmed so that it can control all necessary features of the lock-in amplifier. Following the development of the program, a custom photodetection circuit needs to be designed. The circuit should accommodate the sensors and lock-in amplifier. Lastly, an **Open Lock-In Amplifier (OLIA)**² circuit needs to be tested and compared to conventional lock-in systems.

3.3 Assignment specifications

As already explained, the assignment is quite broad and involves both hardware and software, causing the need for a number of different tools.

Most of the hardware tools are already available at the Applied Nanotechnology lab. The lock-in amplifiers which will be used for the tests are the most important pieces of hardware. Zurich Instruments HF2LI is the benchmark lock-in amplifier. The target amplification is at least 10dB. There are also several different photodetectors available and the one which fits the project best will be picked at a later date. Chapter 3.1 already discussed the basics of the **CW-ODMR** protocol. In order to get an operational **CW-ODMR** setup, an **MW** generator and a laser will be used. **MW** sweeping needs to be done in the range of 2,8 to 2,9 GHz and the lab already has a custom-built **MW** generator that can output these frequencies. The laser is mostly outside the scope of the assignment, as it is almost entirely optical in nature. Setting it up, together with the **NV** samples, is up to the client. However, it is important to note that the fluorescence wavelength should be in the range of 637 to 800 nm, as it plays an important part in reading the **CW-ODMR** data.

In terms of software, there is more freedom of choice. Interfacing with the HF2LI is done through proprietary software, but this is the only required program. There are various **Electronic Computer-Aided Design (ECAD)** software suites that offer the same base functionality. KiCad was selected because the client prefers open-source software. The program for retrieving data from the lock-in amplifiers can be written in both Python and MATLAB. Both languages have good integration with the main lock-in amplifier. They also offer **Graphical User Interface (GUI)** programming capabilities and are good for scientific computing overall.

3.4 Scope of work

3.4.1 Project boundaries

The project boundaries were initially based on the assignment form, but were later discussed with the client and refined further.

Must have

- Hardware platform for photodetection
- Software for signal processing and visualization

Should have

- Tests with different diamond samples

Could have

- Tests with different quantum protocols
- **OLIA** implementation
- Tests comparing **OLIA** to market solutions

Will not have

- Laser as a part of the hardware platform
- Driver upgrade

²**OLIA** is an open-source microcontroller-based lock-in amplifier. It uses common components, which makes it easy to build [6]

3.4.2 Goals

Based on the MoSCoW priorities from Chapter 3.4.1, a set of goals was created to further specify all items from each prioritization category. Every goal was designed so that its outcome results in a tangible project milestone (e.g. a deliverable).

Goal 1 : Create a hardware setup, which measures and amplifies photodiode signals

Goal 2 : Develop software to process and visualize lock-in amplifier signals

Goal 3 : Compare the performance of different lock-in amplifiers

While these goals are practical, they are still not specific enough. To eliminate the possibility of confusion, a set of tasks were created. All tasks contribute to one of the three goals.

Task 1.1 : Design a photodiode **Printed Circuit Board (PCB)**, which can accommodate different lock-in amplifiers

Task 1.2 : Build an operable **OLIA**

Task 2.1 : Develop software that acquires signals and is then able to visualize them

Task 3.1 : Use key performance metrics to compare the **OLIA** implementation to market solutions

Task 3.2 : Measure **OLIA** performance using different diamond samples and quantum protocols

Task 1.1 involves the design and production of a photodiode **PCB**. The **PCB** has to output signals that are not only compatible with lock-in amplifiers that are available on the market, but also with the **OLIA**. This part of the hardware design has the highest priority, which is why it will be done first.

Task 1.2 is to build an **OLIA** amplifier, which can be used at Applied Nanotechnology's laboratory. This will be done with the technical specifications and firmware provided by Harvie and de Mello [6]. The necessity for an **OLIA** is low, because the Applied Nanotechnology research group already has two lock-in amplifiers.

Task 2.1 is to write an application in Python or MATLAB. This can be done on a different setup, but ideally it will use the hardware setup from **Goal 1**. Because the **OLIA** project uses open-source firmware that differs from proprietary solutions, there might need to be two separate applications. This task can only be completed once a measurement setup is built, so its execution will follow the first two tasks.

Task 3.1 requires all previous tasks to be finished. The completed setup needs to be used to measure the performance of lock-in amplifiers available on the market and the **OLIA** implementation. **Signal-to-Noise Ratio (SNR)**, bandwidth and stability are the main metrics that need to be compared.

Task 3.2 is similar to **Task 3.1**, but it is a much broader exploration of the performance of the lock-in amplifiers. Using different diamond samples and quantum protocols will show how the amplifier performs and how different conditions affect it. Because the task can be used to verify the setup from **Goal 1**, it can also be done before **Task 3.1**. Tests with varying diamond samples are more important to the client, which is why they will take precedence over tests with different quantum protocols.

3.4.3 Deliverables

The description of the tasks already provided context for the deliverables, but this subsection contains a formalized version of the deliverables.

1. Photodetection **PCB**
2. **OLIA** implementation
3. Software application
4. Comparison visualization
5. Technical documentation

The only deliverable, which was not mentioned in Chapter 3.4.2 is the technical documentation. This is because it should contain information about every task.

3.5 Methodology

The V-Model methodology was selected, as it is well-suited for low-level projects. Figure 3.2 shows a diagram of the phases of the V-Model. Unlike some software-oriented models, the V-Model is very sequential. This can sometimes be seen as detrimental, but in this case it helps with structuring the project. Another benefit of this model is that there are multiple testing activities, which underpin the quality assurance. A contentious feature of the V-Model is the heavy reliance on the initial requirements. This need for deliberate project requirements can be hard to meet, especially if the client representative is not technically proficient. However, this is not the case in this project. The requirements were extensively discussed with the client representative, based on which the project boundaries in Chapter 3.4.1 were set up.

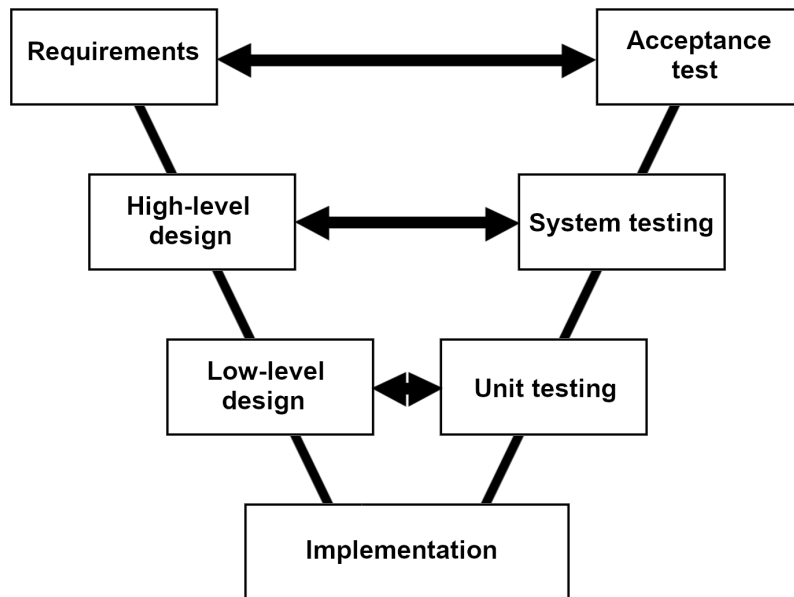


Figure 3.2: V-Model diagram

3.6 Report outline

Chapter 4

Functional design

4.1 Background knowledge

4.1.1 Spin states

Spin, at least in quantum mechanics, is the intrinsic angular momentum of a particle, which is described by the quantum number of the particle. Importantly, it differs from the angular momentum in classical mechanics, which is extrinsic. Spin characterizes systems of particles, usually electrons, using quantum entanglement. This phenomenon refers to the "entanglement", or spin correlation, of a set of particles.

These foundational concepts make it possible to describe quantum systems using various states. The most simple states, used as descriptors, are the energy states. Ground states refer to the system being in an energy minimum. On the other hand, excited states signify that the system has more energy than at its ground state. Additionally, there can be intermediate states during state transition.

While the aforementioned states describe system energy, they have no bearing on the spin. For the purposes of this project, only two spin states need to be explained. The first one is called singlet state. It occurs when an entangled system has a total spin of 0, caused by the mutual cancellation of spin. For example, for a system of two entangled electrons to be a singlet, the two spins would need to point in opposite directions. The second spin state is called triplet and it has a total spin of 1. Triplets can consist of, for instance, two unpaired electrons with aligned spins that sum up to 1. Singlets and triplets both have major distinguishing features and properties, which is why they can be used for quantum sensing. Aside from the difference in spin, triplets tend to have higher energy levels. They also exhibit attraction to magnetic fields, while singlets cannot be influenced directly by magnetism.

4.1.2 Zeeman effect

Discovered by Pieter Zeeman in 1896, the Zeeman effect is another important phenomenon that enables quantum sensing. If under normal circumstances a light-emitting quantum system only emits one spectral line, then when a magnetic field is applied to it the line will split, thus exhibiting the Zeeman effect. In an NV center, this phenomenon causes the $|\pm 1\rangle$ energy level to split into $|+1\rangle$ and $| -1\rangle$.

4.1.3 Energy levels

Figure 4.1 shows the energy level diagram of an NV center.

After illuminating the NV center with a green laser, electrons go from a ground state to an excited state. They then need to return to the ground state. This decay process is usually direct and emits a red photon, however it can also go through the metastable singlet state and emit an infrared photon. It should be noted that whenever the NV center is exposed to the resonant frequency $\nu = 2,87\text{GHz}$ the probability of emitting an infrared photon is significantly increased.

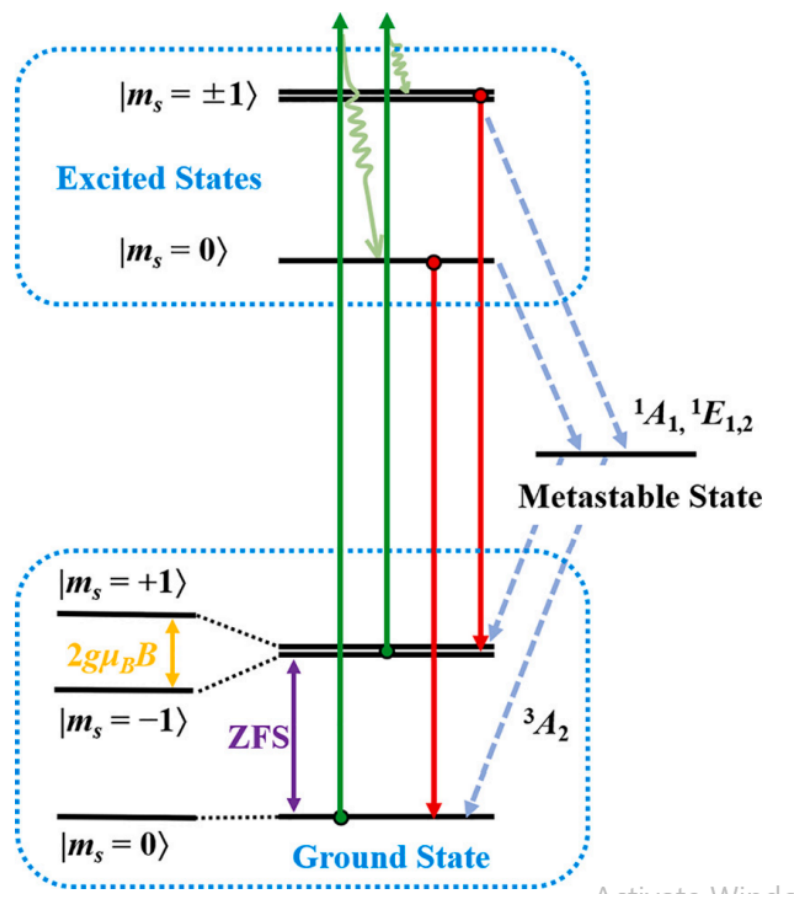


Figure 4.1: NV center energy level diagram (image credit to Song et al [7])

4.2 Quantum protocols

There are a number of different quantum protocols, which differ in what they can measure, in how precisely they can measure it and in the complexity of the hardware they require to operate. **CW-ODMR** is the main protocol this project is aimed at facilitating. As Saijo et al [8] demonstrate, CW-ODMR is relatively simple, while still detecting magnetic field with reasonable sensitivity. P-ODMR does outperform CW-ODMR [9], but because of the added complexity working with it is a "Could have" (see Chapter 3.4.1). Before being able to run P-ODMR on the setup at the lab, several protocols need to be implemented first [4]. T_1 measurements, which are one of the fundamentals of **Magnetic Resonance Imaging (MRI)**, should be conducted first. Afterwards, Rabi oscillations need to be observed and measured in order to calibrate the setup. Without these intermediate protocols, P-ODMR cannot be performed.

4.2.1 CW-ODMR

CW-ODMR is a quantum protocol that has seen extensive usage in sensing setups that measure magnetic fields. Its working principle is centered around the photoluminescence of NV centers and the difference in light emission based on spin states. As already discussed in Chapter 4.1.3, the NV center emits less visible light when at the resonant frequency ν . Additionally, two more dips appear on the spectrum if a magnetic field is applied. Calculating the magnetic field can be done using the formula $h\nu = g_e\mu_B B_{AC}$ ¹. Figure 4.2 shows an example of what a CW-ODMR spectrum might look like.

4.2.2 T_1 relaxometry

T_1 , T_2 and T_2^* relaxation time measurements are commonly associated with radiometry [10], but they have other uses too. T_1 measurements, in particular, are useful in the realm of quantum

¹3, In the formula, h is the Planck constant, g_e is the g-factor of the electron and μ_B is the Bohr magneton. Knowing all other variables, B_{AC} can easily be calculated.

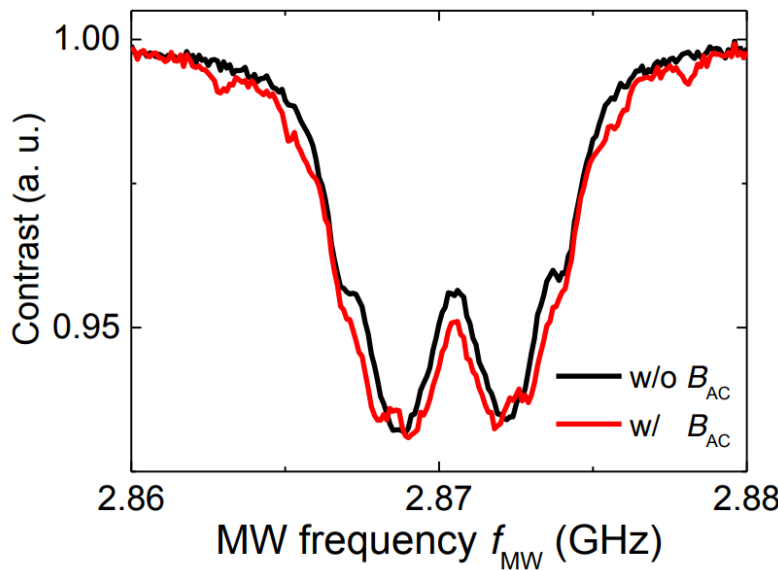


Figure 4.2: Example of a CW-ODMR spectrum **with** and **without** a magnetic field (image credit Saijo et al [8])

sensing. Knowing the T_1 relaxation time, which refers to the time it takes for the spins in an NV system to decay back to their original state, makes it possible to adjust the pulse sequences of more complex protocols and thus get better results.

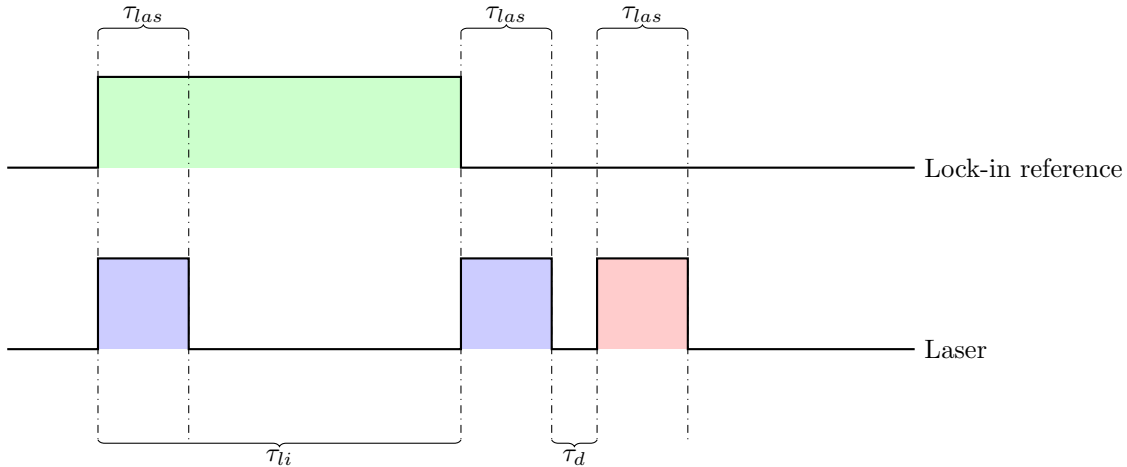


Figure 4.3: Laser and reference signals for T_1 measurements

The waveforms which are needed for T_1 measurements are shown in Figure 4.3. While both are important in practice, the lock-in is not as relevant, at least in this section of the report. However, its working principle is explored in Chapter 4.4. For now, all that needs to be said about the lock-in reference signal is that it is periodic and τ_{li} is much longer than τ_{las} (Sewani et al [4] propose $\tau_{li} = 15ms$ and $\tau_{las} = 5\mu s$). Laser pulses, on the other hand, are not periodic. Instead, there are three short pulses every reference period (which is $2\tau_{li}s$ long). The two blue pulses have the same timing every cycle, because they initialize the NV spins. However, the red pulse always occurs after the variable dark time τ_d . Depending on the T_1 decay at the time of the readout pulse, a different voltage will be detected. Figure 4.4 shows what results can be expected when measuring T_1 . Determining the value of T_1 is done using Formula 4.1, where I is the light intensity, I_∞ is the light intensity offset and τ_d is the dark time.

$$I(t) = I_\infty + I(0)e^{-\tau_d/T_1} \quad (4.1)$$

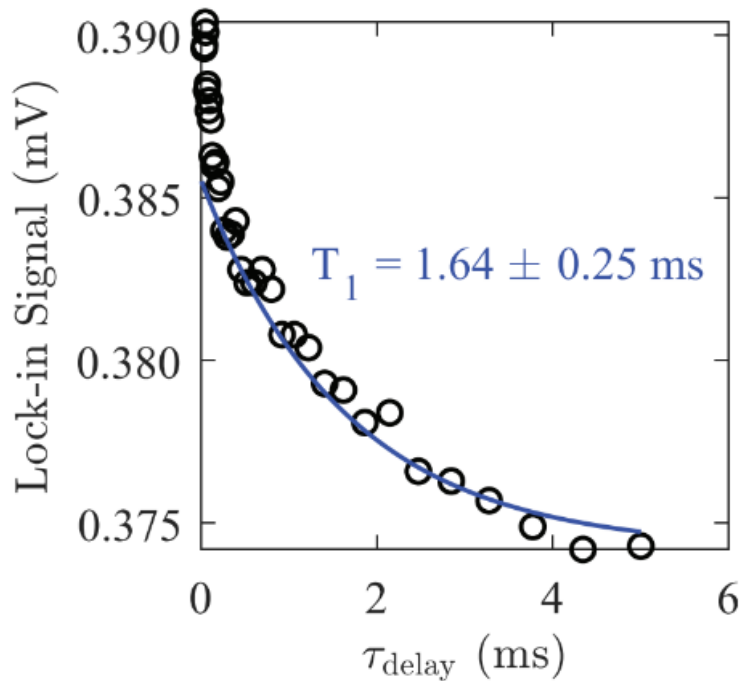


Figure 4.4: Results of a set of T_1 measurements with varied dark time τ_d (image credit to Sewani et al [4])

4.2.3 P-ODMR

As a descriptor **P-ODMR** is somewhat vague, which is why it has been used for a number of protocols. Different pulse schemes can result in radically different . Some researches use

4.3 Quantum sensing setup

Executing all of the aforementioned protocols requires a sensing setup with some specific capabilities. This section discusses the devices that make up the setup and the functionalities required by each protocol.

A high-level diagram of the quantum sensing system can be seen in Figure 4.5. There are 2 input devices in the system, but most protocols exclusively use the function generator. On the other hand, only a single lock-in amplifier is used as an output device for all measurements.

The blue boxes show the components responsible for sending and receiving light signals. They constitute the core of the setup. Waveforms are generated by the function generator, no matter the protocol. Using a current driver, the laser is then used to illuminate the diamond sample. The resulting luminescence is then measured by the photodetector and processed by the lock-in amplifier. All protocols need this part of the setup, however they utilize it differently.

Microwave generation, when needed, starts with a **TTL** signal from the function generator or a frequency sweep using a dedicated device. Out of all protocols, only **CW-ODMR** requires a sweep. The antenna then broadcasts the signal, while the switch isolates the signal generator from it.

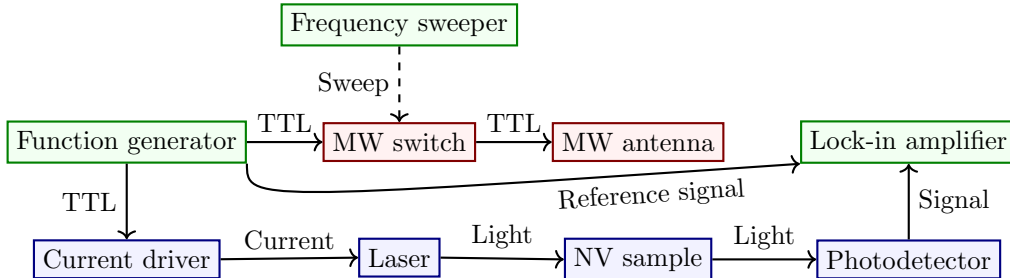


Figure 4.5: High-level overview of the quantum sensing setup

4.4 Lock-in amplification

As a means of retrieving data, lock-in amplification is the most suitable for the setup due to its relatively low cost, signal retrieval capabilities and the possibility of using one amplifier for several setups.

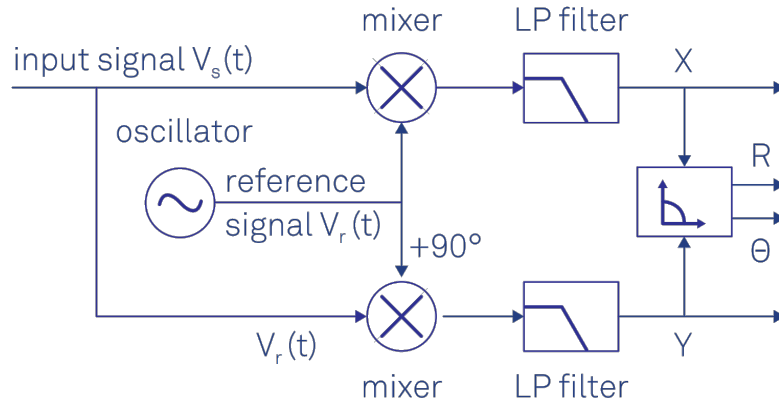


Figure 4.6: High-level diagram of a lock-in amplifier (image credit to Zurich Instruments [11])

Figure 4.6 shows an overview of how lock-in amplification works. Simply put, the amplifier receives a signal V_s and extracts the data at the frequency of a reference signal V_r . To explain this more thoroughly, lock-in amplification utilizes the fact that every signal is made of periodic waves, which are equal to zero when averaged.

$$V_s = R \cos(\omega_s t + \theta) = \frac{R}{2} e^{i(\omega_s t + \theta)} + \frac{R}{2} e^{-i(\omega_s t + \theta)} \quad (4.2)$$

Equation 4.2 shows how the mathematical expression of a sine wave signal, where ω_s is the frequency and θ is the phase of the signal. Using the trigonometric identity $\cos x = \frac{1}{2}(e^{ix} + e^{-ix})$, the signal can be represented in terms of complex numbers.

$$V_r = e^{-i\omega_r t} \quad (4.3)$$

In Equation 4.3, a simplified reference signal is shown. Real applications might require more complex reference signals, but V_r is perfect for demonstrating the lock-in principle.

$$V_m = V_s V_r = \frac{R}{2} e^{i(\omega_s - \omega_r)t + \theta} + \frac{R}{2} e^{-i(\omega_s + \omega_r)t + \theta} \quad (4.4)$$

Finally, Equation 4.4 shows the product of the signal V_s and the reference V_r . In the case of $\omega_s = \omega_r$, there is a signal at 0 Hz and another one at $2\omega_s$ Hz. The latter, however, should be attenuated to an undetectable level by the low-pass filters shown in Figure 4.6. This way, both the unwanted signal appearing at double the frequency and all of the noise at different frequencies is attenuated.

4.5 Photodetection

Photodetection is how the NV photoluminescence is measured, effectively turning light into current using a photodiode. However, a bare photodiode cannot be connected to a lock-in amplifier, because it functions as a current generator. This is where the photodetection PCB comes in. Its purpose is to transform the current into voltage and then amplify the resulting signal to the necessary voltage level.

4.6 Photodiodes

At the heart of the photodetector lies the photodiode. It is what turns light into current and drives the Transimpedance Amplifier (TIA) that follows it. While the specifications of the diode are not the most important part of the photodetector circuit, they still need to be discussed, due to the impact the two ways of biasing can have on the circuit.

An exceedingly common photodiode configuration,

4.6.1 Design process

Designing the photodetector is mostly about creating a **TIA**, which is a tool used for converting current to voltage, and specifically tuning its parameters so that it works with the selected photodiode under operating conditions.

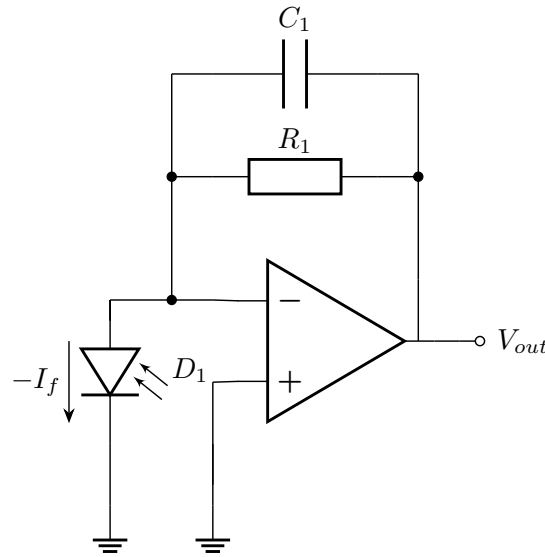


Figure 4.7: Basic **TIA** circuit

The basic circuit, shown in Figure 4.7, is all that is required for photodetection. Following the guidelines for making a **TIA** set by Texas Instruments [12], all the parameters of the circuit can be calculated.

$$R_1 = \frac{V_{o \ max}}{I_{o \ max}} \text{ assuming } V_{o \ min} = 0V \quad (4.5)$$

The resistor R_1 determines the transimpedance gain of the amplifier. Equation 4.5 shows how its value can be calculated by using the output voltage and input current. It should be noted that the minimum output voltage is always 0 in this use case.

$$C_1 = \frac{1}{2\pi R_1 f_{rc}} \quad (4.6)$$

The capacitance of C_1 can be calculated using the resistance of R_1 and the cutoff frequency f_{rc} , as shown in Equation 4.6.

In addition, a non-inverting amplifier can be added, to increase the gain of the circuit even more, without affecting the phase. Figure 4.8 shows how it can be connected to the output of the **TIA** from Figure 4.7.

Equation 4.7 is used to calculate the gain of second amplification stage. The formula is derived from the voltage divider formed by the two resistors and the fact that $V_{ot} = V_-$.

$$A_{nia} = \frac{V_{out}}{V_{ot}} = 1 + \frac{R_3}{R_2} \quad (4.7)$$

The design is based on circuits provided by the client. At their request, the first version of the PCB is an exact replica of the original circuit.

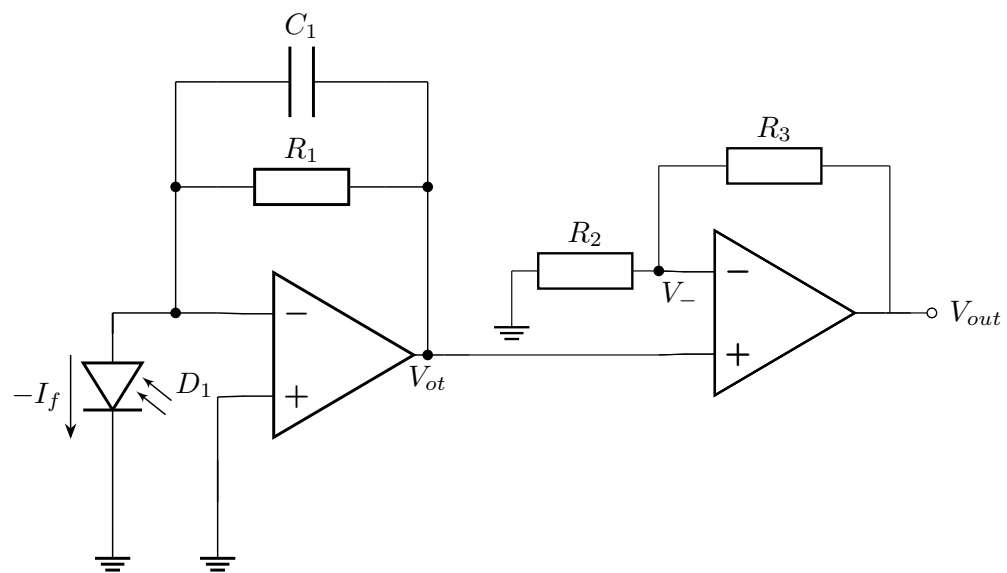


Figure 4.8: TIA with non-inverting output amplification

Chapter 5

Technical design

5.1 Quantum sensing setup

5.2 Photodetector design

As an integral part of the sensing setup, the photodetector needs a lot of attention. Good amplification is crucial to increasing the **SNR** of the quantum setup. Based on the design ideas presented in the functional design (see Chapter 4.6.1), the photodetection circuit can be drawn up.

5.2.1 First iteration

As previously mentioned, the first iteration of the PCB uses component values provided by the client. There is no specific information for the design process, aside from the fact that the original designer made the photodetector for input currents in the range of several nanoamperes. Such low inputs require high R_1 values, however increasing the resistor value results in more biasing current going to the amplifier and a more limited dynamic range [13]. Furthermore, it is entirely possible that the original design did not thoroughly consider the bandwidth needed for different protocols, as **CW-ODMR** setups do not require broad bandwidths [14]. Biasing is another concern with this photodiode setup. The configuration shown in Figures 4.7 and 5.1 has the diode in the photovoltaic mode, which is suitable for low-frequency, low-light operation. In spite of this setup being suited to **CW-ODMR**, pulsed protocols require micro to nanosecond precision

5.2.2 Second iteration

Building on the time-domain analysis in the previous chapters, a frequency-domain analysis can help fill in the gaps [15–17].

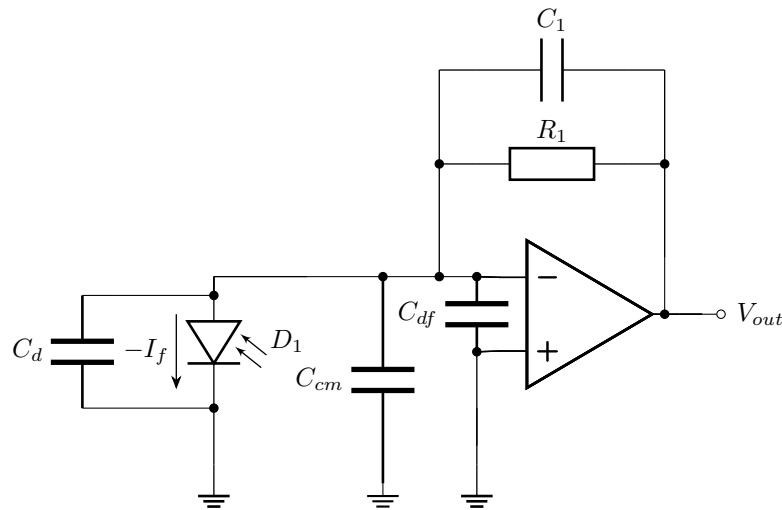


Figure 5.1: Parasitic capacitances in a **TIA** circuit

Introducing the real-world parasitic capacitances to the ideal TIA shown in Figure 4.7 results in the circuit in Figure 5.1. The diode capacitance C_d , combined with the differential and common-mode capacitances of the amplifier (C_{df} and C_{cm}), contributes a significant amount of capacitance to the circuit and can result in instability [18].

$$C_i = C_d + C_{df} + C_{cm} \quad (5.1)$$

The combined input capacitance (Equation 5.1) is needed when solving the equation arising from **Kirchhoff's Current Law (KCL)** at the inverting input of the amplifier. Z_1 (Equation 5.2), or the combined impedance of R_1 and C_1 , is another prerequisite for deriving the transimpedance Z_t using **KCL**. Additionally, the open-loop gain A_{ol} is needed for the derivation of the transimpedance. Equation 5.3 shows the open-loop gain, expressed with the **Direct Current (DC)** open-loop gain A_o and the open-loop cutoff frequency ω_s , which is equivalent to $\frac{v_{out}}{v_{in}}$.

$$Z_1(s) = \frac{1}{\frac{1}{R_1} + sC_1} \quad (5.2)$$

$$A_{ol}(s) = A_o \frac{\omega_0}{s + \omega_0} = \frac{v_{out}}{v_{in}} \quad (5.3)$$

Finally, the values in the **KCL** equation (Equation 5.4) can be substituted, from which Z_t can be derived, as seen in Equation 5.5.

$$i_f = \frac{v_i}{\frac{1}{sC_i}} + \frac{v_{in} - v_{out}}{Z_1(s)} \quad (5.4)$$

$$\begin{aligned} Z_t(s) &= \frac{v_{out}}{i_f} \\ &= \frac{A_o \omega_o R_1}{s^2 R_f (C_i + C_f) + s(1 + \omega_o R_1 C_1 (1 + A_o) + \omega_o R_1 C_i) + \omega_o (1 + A_o)} \\ &= A_{ol}(s) \frac{Z_f}{1 + A_{ol}(s) + s C_i Z_f} \end{aligned} \quad (5.5)$$

Before moving on to the pole analysis, the impact of the quality factor Q on the system response should be considered. Two system poles present when $Q > 0, 5$. For $Q = \frac{\sqrt{3}}{3}$, the system has a Bessel response, which has the flattest group delay, however, if $Q = \frac{\sqrt{2}}{2}$, then the system has a Butterworth response, which means it has the flattest possible amplitude response. Although the group delay is not as important as the amplitude response, a Bessel response also results in smaller amount of overshoot and less jitter, which is why it is preferred.

$$H(s) = H_0 \frac{(-s_1)(-s_2)}{(s - s_1)(s - s_2)} = G_0 \frac{s_1 s_2}{s^2 + s(-s_1 - s_2) + s_1 s_2} \quad (5.6)$$

Based on this consideration, the poles can be found using the general form of a second order transfer function, shown in Equation 5.7.

$$\begin{aligned} -s_1 - s_2 &= \frac{1 + \omega_o(C_i + (1 + A_o)C_1)R_1}{(C_i + C_1)R_1} \\ s_1 s_2 &= \frac{\omega_o(1 + A_o)}{(C_i + C_1)R_1} \end{aligned} \quad (5.7)$$

At this point in the design process, the values of R_1 and C_1 need to be considered again.

5.3 Photodetection implementation

Implementing the photodetectors is as much about the creation of a physical board, as it is about simulating the circuits that are presented in Chapter 5.2.

5.3.1 First iteration

Figure 5.2 shows the LTSpice design. C_1 and R_2 , as well as the current source I_1 are used to simulate the behavior of a photodiode.

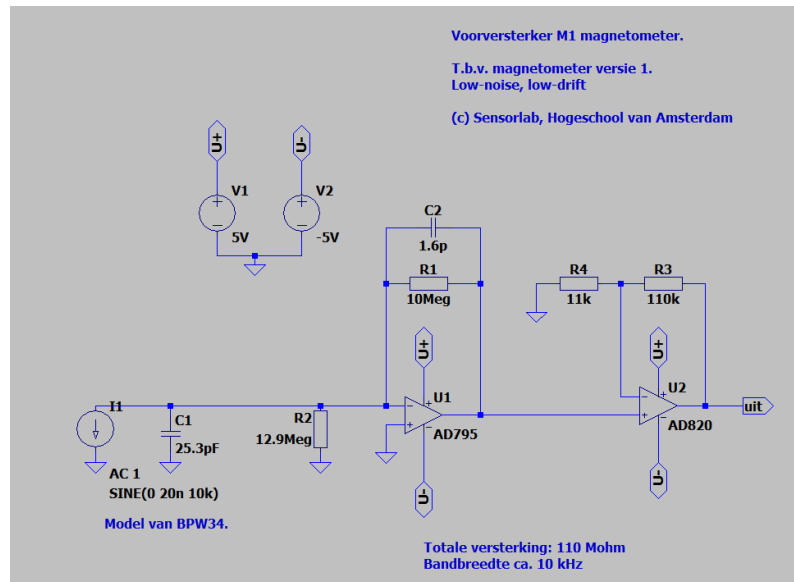


Figure 5.2: Provided photodetector design

Simulation

Tina-TI was used to simulate and visualize the DC gain and frequency response of the system, as seen in Figure 5.3. The signals V_{ot} and V_{out} correspond to the output of the transimpedance and non-inverting amplification stage respectively. The AC plot (Figure 5.3a) shows the cutoff, at 10,77 kHz, and the gain inside the gain bandwidth, which is 160,82 dB. The DC plot (Figure 5.3b) shows the voltage with respect to the current and demonstrates the linearity of the system in the range of 0 to 46,31 nA. After V_{out} reaches 5 V, the output remains fixed, because it cannot exceed the voltage provided to the amplifier.

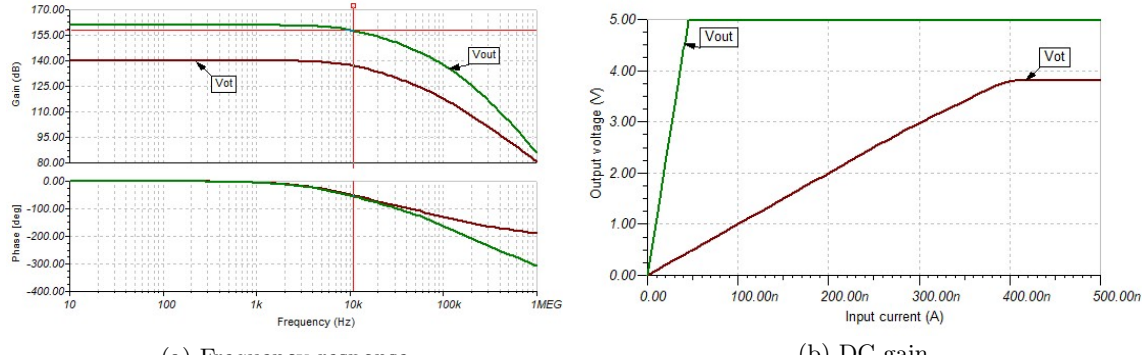


Figure 5.3: Simulation of the first iteration of the photodetector

Implementation

Figure 5.4 shows the back side of the PCB. It hosts all components, except for the photodiode, which sits unobstructed on the front side. Requirements for the physical dimensions were also set by the client. The PCB needs to fit the Thorlabs mount standard, since the rest of the setup also uses it.

5.4 OLIA implementation

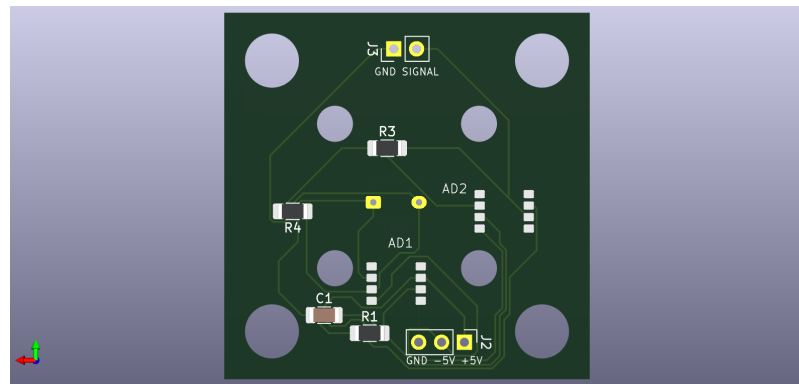


Figure 5.4: First iteration of the photodetection PCB

Chapter 6

Testing results

Number	Task	Status
1.1	Deploy and configure at least one OpenRemote instance	Completed
1.2	Establish communication to the OpenRemote instance using the HTTP and MQTT protocols	Completed
2.1	Simulate IoT devices (smart homes) that send and receive concurrent MQTT data to OpenRemote and measure the latency of the transmissions	Completed
2.2	Create a physical IoT device setup using a platform like ESP32 or Arduino and recreate the tests from Goal 1.2	Completed
2.3	Integrate and test OpenRemote's Prophet project	Not started
2.4	Test performance and create visualizations	Completed
3.1	Document technical progress	Completed
3.2	Reflect on personal and professional development	Completed
3.3	Communicate project results	Ongoing

Table 6.1: Goal completion

6.1 Test goals and performance metrics

Metric	API	Unit(s) of measurement	Explanation
Device provisioning latency	HTTP	seconds (s)	Time between creation request and confirmation
Message loss percentage	MQTT	percent (%)	Percent of MQTT messages which are lost
Resource usage	-	percent (CPU %, RAM %)	CPU and RAM usage when running tests

Table 6.2: Metrics of the OpenRemote scalability tests

6.2 Test setup**6.3 Results and discussion****6.4 Known limitations**

Chapter 7

Conclusion

Chapter 8

Recommendations

Appendix A

Code

Glossary

DC Direct Current 17

ECAD Electronic Computer-Aided Design 6

GUI Graphical User Interface 6

KCL Kirchhoff's Current Law 17

MRI Magnetic Resonance Imaging 10

MW Microwave 5, 6

NV Nitrogen Vacancy 5, 6, 9–11, 13

ODMR Optically Detected Magnetic Resonance 5, 25

CW-ODMR Constant-Wave ODMR 5, 6, 10–12, 16

P-ODMR Pulsed ODMR 5, 10, 12

OLIA Open Lock-In Amplifier 6, 7

PCB Printed Circuit Board 7, 13

SNR Signal-to-Noise Ratio 7, 16

TIA Transimpedance Amplifier 13–17

TTL Transistor-Transistor Logic 5, 12

Bibliography

- [1] Wikipedia contributors, *Nitrogen-vacancy center — Wikipedia, the free encyclopedia*, [Online; accessed 3-September-2025], 2025. [Online]. Available: https://en.wikipedia.org/w/index.php?title=Nitrogen-vacancy_center&oldid=1301369588.
- [2] Wikipedia contributors, *Photoluminescence — Wikipedia, the free encyclopedia*, <https://en.wikipedia.org/w/index.php?title=Photoluminescence&oldid=1309081879>, [Online; accessed 4-September-2025], 2025.
- [3] Wikipedia contributors, *Optically detected magnetic resonance — Wikipedia, the free encyclopedia*, https://en.wikipedia.org/w/index.php?title=Optically_detected_magnetic_resonance&oldid=1301371272, [Online; accessed 6-October-2025], 2025.
- [4] V. K. Sewani et al., “Coherent control of nv- centers in diamond in a quantum teaching lab,” *American Journal of Physics*, vol. 88, no. 12, pp. 1156–1169, 2020.
- [5] A. Haque and S. Sumaiya, “An overview on the formation and processing of nitrogen-vacancy photonic centers in diamond by ion implantation,” *Journal of Manufacturing and Materials Processing*, vol. 1, no. 1, p. 6, 2017.
- [6] A. J. Harvie and J. C. de Mello, “Olia: An open-source digital lock-in amplifier,” *Frontiers in Sensors*, vol. 4, p. 1102176, 2023.
- [7] Z. Song et al., “Enhancing fluorescence of diamond nv- centers for quantum sensing: A multi-layer optical antireflection coating,” *Diamond and Related Materials*, vol. 141, p. 110584, 2024.
- [8] S. Saijo et al., “Ac magnetic field sensing using continuous-wave optically detected magnetic resonance of nitrogen-vacancy centers in diamond,” *Applied Physics Letters*, vol. 113, no. 8, 2018.
- [9] Y. Zhang et al., “High-sensitivity dc magnetic field detection with ensemble nv centers by pulsed quantum filtering technology,” *Optics Express*, vol. 28, no. 11, pp. 16191–16201, 2020.
- [10] J. Jones, W. Howden, A. Murphy, et al., *T1 relaxation time*. [Online]. Available: <https://doi.org/10.53347/rID-25821>.
- [11] Z. Instruments, “Principles of lock-in detection and the state of the art. 2016,” *Internetadresse: https://www.zhinst.com/sites/default/files/li_primer/zi_whitepaper_principles_of_lock-in-detection.pdf*. Zuletzt aufgerufen am, vol. 17, 2018.
- [12] P. Semig, *Transimpedance amplifier circuit*. [Online]. Available: <https://www.ti.com/lit/an/sboa268b/sboa268b.pdf>.
- [13] B. Black and G. Brisebois, *Transimpedance amplifiers for wide range photodiodes have challenging requirements*, 2021.
- [14] B. Acharya, “Compact integration of nv-based diamond quantum sensors using a small-size photodiode and on-board transimpedance amplifier,” Ph.D. dissertation, Wichita State University, 2025.
- [15] E. Margan, “Transimpedance amplifier analysis,” *no*, vol. 1, pp. 1–19, 2012.
- [16] E. Säckinger, *Analysis and design of transimpedance amplifiers for optical receivers*. John Wiley & Sons, 2017.
- [17] L. Horsthemke et al., “All optical magnetometry with nitrogen vacancy centers in diamonds,” Ph.D. dissertation, Universidad de Granada, 2025.
- [18] S. Cherian, “What you need to know about transimpedance amplifiers—part 1,” *Texas Instruments Incorporated*, 2016.